

Research article

Izabela Kaminska^a, Carolin Vietz^a, Álvaro Cuartero-González, Philip Tinnefeld, Antonio I. Fernández-Domínguez and Guillermo P. Acuna*

Strong plasmonic enhancement of single molecule photostability in silver dimer optical antennas

<https://doi.org/10.1515/nanoph-2017-0081>

Received August 24, 2017; revised October 27, 2017; accepted November 21, 2017

Abstract: Photobleaching is an effect terminating the photon output of fluorophores, limiting the duration of fluorescence-based experiments. Plasmonic nanoparticles (NPs) can increase the overall fluorophore photostability through an enhancement of the radiative rate. In this work, we use the DNA origami technique to arrange a single fluorophore in the 12-nm gap of a silver NP dimer and study the number of emitted photons at the single molecule level. Our findings yielded a 30× enhancement in the

average number of photons emitted before photobleaching. Numerical simulations are employed to rationalize our results. They reveal the effect of silver oxidation on decreasing the radiative rate enhancement.

Keywords: photon count enhancement; reduction of photobleaching; DNA origami; single-molecule detection; plasmonics; silver nanoparticle.

1 Introduction

Nanostructured metals affect the photophysical properties of luminescent molecules placed in close proximity [1]. In particular, the interaction of fluorescent molecules and metallic nanoparticles (NPs) has been intensely studied over the last decades [2]. Positioning NPs and single fluorescent molecules with nanometric precision enabled the fabrication of optical antennas (OAs) capable of enhancing and directing photon absorption and emission [3, 4]. Most works have focused on the capacity of OAs to concentrate propagating radiation into sub-wavelength volumes to enhance the fluorescence intensity (i.e. the photon count rate) of fluorophores, mostly through an increment of the excitation rate [5]. Fewer studies have addressed the function of OAs in emission [6], where they can modulate the radiative and non-radiative decay rates, as well as the directionality of fluorescence [7]. Remarkably, the effect of OAs on the average number of emitted photons ($\langle n \rangle$) has been largely overlooked, with a few works focusing on single-particle OAs with rather low fluorescence enhancement [8, 9].

The total number of fluorescence photons that a molecule can emit is typically limited by photobleaching, i.e. irreversible photochemical reactions occurring from the excited state. Therefore, enhancing the radiative rate reduces the time spent in an excited state, and hence, a higher radiative rate increases the total number of fluorescence photons. In addition, other strategies to increase photostability include the use of OAs to reduce the time spent in long-lived states such as triplet states [10]. This

***Izabela Kaminska and Carolin Vietz:** These authors contributed equally to this work.

***Corresponding author: Guillermo P. Acuna**, Institute for Physical and Theoretical Chemistry, and Braunschweig Integrated Centre of Systems Biology (BRICS), and Laboratory for Emerging Nanometrology (LENA), Braunschweig University of Technology, Rebenring 56, 38106 Braunschweig, Germany, e-mail: g.acuna@tu-bs.de

Izabela Kaminska: Institute for Physical and Theoretical Chemistry, and Braunschweig Integrated Centre of Systems Biology (BRICS), and Laboratory for Emerging Nanometrology (LENA), Braunschweig University of Technology, Rebenring 56, 38106 Braunschweig, Germany; and Institute of Physics, Faculty of Physics, Astronomy, and Informatics, Nicolaus Copernicus University, Grudziadzka 5, 87-100 Torun, Poland

Carolin Vietz: Institute for Physical and Theoretical Chemistry, and Braunschweig Integrated Centre of Systems Biology (BRICS), and Laboratory for Emerging Nanometrology (LENA), Braunschweig University of Technology, Rebenring 56, 38106 Braunschweig, Germany

Álvaro Cuartero-González and Antonio I. Fernández-Domínguez: Departamento de Física Teórica de la Materia Condensada and Condensed Matter Physics Center (IFIMAC), Universidad Autónoma de Madrid, E-28049 Madrid, Spain

Philip Tinnefeld: Institute for Physical and Theoretical Chemistry, and Braunschweig Integrated Centre of Systems Biology (BRICS), and Laboratory for Emerging Nanometrology (LENA), Braunschweig University of Technology, Rebenring 56, 38106 Braunschweig, Germany; and Department Chemie, Ludwig-Maximilians-Universität München, Butenandtstr. 5-13 Haus E, 81337 München, Germany

is a key function of OAs, as the amount of information obtainable from a fluorescence measurement is determined by the total number of detected photons.

Perhaps the main reason behind the lack of experimental studies on the effect of OAs on the photostability of single molecules lies in the fact that measurements are intrinsically demanding. Photobleaching is a stochastic process, and in ideal cases, the total number of emitted photons by a set of fluorophores follows an exponential probability distribution. At low excitation intensity, multi-photon contributions to photobleaching are small and the number of emitted photons is in first approximation independent of excitation intensity. In order to determine $\langle n \rangle$, the exponential distribution has to be fully characterized, which involves the following challenges. Estimation of fluorescence enhancement induced by an OA was achieved by fluorescent correlation spectroscopy (FCS) measurements from molecules diffusing through the hotspot providing preliminary insight [11]. However, the determination of $\langle n \rangle$ involves the realization of single molecule measurements until the occurrence of a photobleaching event. Furthermore, during this photobleaching time, which can take up to several minutes, the distance between the OAs and the single fluorophores has to be adjusted with nanometer accuracy and stoichiometric control. Over the last years, the DNA origami technique has been exploited to circumvent these challenges. This approach, which can be employed to self-assemble different species such as fluorophores and NPs with nanometer accuracy and stoichiometric control, has enabled several experimental studies on the interaction between single fluorophores and OAs [12–15].

In a previous work, we used the DNA origami technique to position a single fluorophore in the vicinity of a gold NP and demonstrated that $\langle n \rangle$ could be enhanced by a factor of 4 [9]. In this contribution, we show that an additional NP can lead to increment of approximately an extra order of magnitude. We built dimer OAs based on 80-nm silver NPs, self-assembled onto a pillar-shaped DNA origami structure in an aqueous environment. Note that silver presents lower absorption losses than gold within the visible range, which, in principle, makes it a better plasmonic material. However, it is also highly more susceptible to oxidation effects, which, in practice, limits the use of silver OAs in non-vacuum conditions [16]. Our experimental results indicate that despite oxidation, a single fluorophore placed at the center of the 12-nm gap between two silver NPs exhibits on average an enhancement in $\langle n \rangle$ of 30 \times . Furthermore, we present numerical simulations that shed insights into the impact that silver

oxidation has on the Purcell effect taking place in the experimental samples.

2 Results and discussion

Figure 1A sketches the OA employed to enhance the photostability of fluorophores. It consists of a pillar-shaped three-dimensional (3D) DNA origami structure. The main shaft is based on a 12-helix bundle, which is thinned at the top to a 6-helix bundle with a diameter of approximately 6 nm. The origami structure is vertically immobilized onto a previously functionalized glass coverslip through biotin modifications at the base. The surrounding consists of an aqueous buffer solution. Two 80 nm in diameter silver NPs are incorporated at the top of the origami structure in order to fabricate OA dimers by DNA hybridization with a set of three capturing strands per NP. Within the nanofabrication protocol followed, samples can contain a distribution of DNA origami structures with two NPs (dimers), a single NP (monomers), and no NP (reference) depending on several parameters such as NP concentration and incubation time. In the 12-nm gap between the NPs, a single fluorophore Alexa488 is incorporated within the DNA

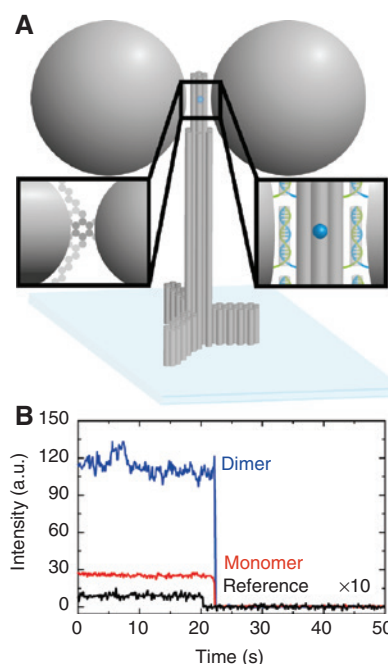


Figure 1: Experimental description.

(A) Sketch of the OA consisting of two 80-nm-diameter Ag NPs self-assembled onto a 3D DNA origami structure. In the 12-nm gap between the NPs, a single fluorophore Alexa488 is positioned. (B) Fluorescence transients extracted from samples A (reference), B (monomers), and C (monomers and dimers).

origami structure. We have recently demonstrated that this silver-based OA dimer can enhance the photon count rate of Alexa488 by two orders of magnitude [17].

Fluorescence measurements were performed with a custom-built wide-field microscope with epifluorescence illumination. We studied three samples, DNA origami structures with no capturing strands (sample A), a single set (sample B), and two sets (sample C) of capturing strands. Sample A cannot incorporate NPs and constitutes the reference. Sample B can incorporate a single NP and consists of a population of monomers and references. Finally, sample C with two sets of capturing strands contains dimers, monomers, and references. A typical fluorescence transient belonging to sample A is included in Figure 1B. Only transients with a single bleaching step were considered to ensure that only single molecules are studied. Monomer and dimer OAs can enhance the photon count rate of the single Alexa488 on average by a factor of 30 and 140, respectively [17], mostly through an increment of the excitation rate. Therefore, in order to avoid saturation [8], samples B and C were studied with five times less excitation power than the reference, sample A. These conditions of low excitation power rendered reference structures with no particle undetectable, and therefore, in sample B, only monomers are detected, while in sample C, both monomers and dimers can be detected. Fluorescence transients from samples B and C are included in Figure 1B.

In order to obtain the total number of photons emitted by each single fluorophore, its emission was recorded until photobleaching occurred. From the fluorescence transients, the total number of emitted photons for each structure was extracted. Figure 2 shows a semi-log histogram plotting the relative number of fluorophores (frequency) versus the number of photons emitted before bleaching. In Figures 2A and B (samples A and B), the probability distributions follow a mono-exponential trend, whereas for sample C (Figure 2C), a bi-exponential dependence is observed. This is in agreement with the type of structures

expected in each sample. For samples A and B, the measured distributions are fitted (black lines) according to the following:

$$P(n) \propto e^{-n/\langle n \rangle}, \quad (1)$$

with n as the number of photons. Following this analysis, the average numbers of emitted photons for the reference (sample A) and the monomer (sample B) are $\langle n_r^A \rangle = (28 \pm 1) \times 10^3$ and $\langle n_m^B \rangle = (110 \pm 10) \times 10^3$, respectively, which translate into a radiative enhancement of $4\times$ for the monomer structure. This number is comparable to our previous report on gold NPs [9].

To account for the two distinct OA structures in sample C (monomers and dimers), the measured frequencies were fitted to a probability distribution containing a sum of two exponential terms

$$P(n) \propto e^{-n/\langle n_m^C \rangle} + \kappa e^{-n/\langle n_d^C \rangle}, \quad (2)$$

where κ is the constant that weighs the number of dimers in the sample. The average numbers of photons obtained for each partial distribution are $\langle n_m^C \rangle = (116 \pm 13) \times 10^3$ and $\langle n_d^C \rangle = (840 \pm 210) \times 10^3$. Note that $\langle n_m^C \rangle$ is in good agreement with $\langle n_m^B \rangle$ and therefore can be safely ascribed to the population of monomers. Thus, $\langle n_d^C \rangle$, which can be assigned to dimer structures, reveals a $30\times$ enhancement in the average number of emitted photons (with respect to the reference sample). To our knowledge, this result constitutes the highest photon number enhancement reported through direct experiments in plasmonic OAs up to date [8, 9].

In contrast to fluorescence enhancement studies where all photophysical rates, i.e. excitation, radiative and nonradiative rates, are influenced, the total number of photons is a direct measure of the radiative rate. Therefore, we can directly compare the changes of the radiative rate with finite element simulations of an emitter next to plasmonic structures. Alternative

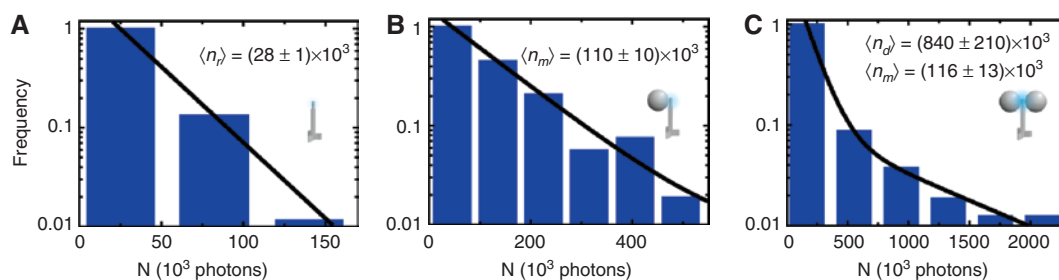


Figure 2: Experimental total number of photons.

Normalized semi-log histogram plot of the total number of photons for samples A, B, and C in (A), (B) and (C), respectively. The black line shows a fit using an exponential distribution (samples A and B) and a bi-exponential distribution (sample C).

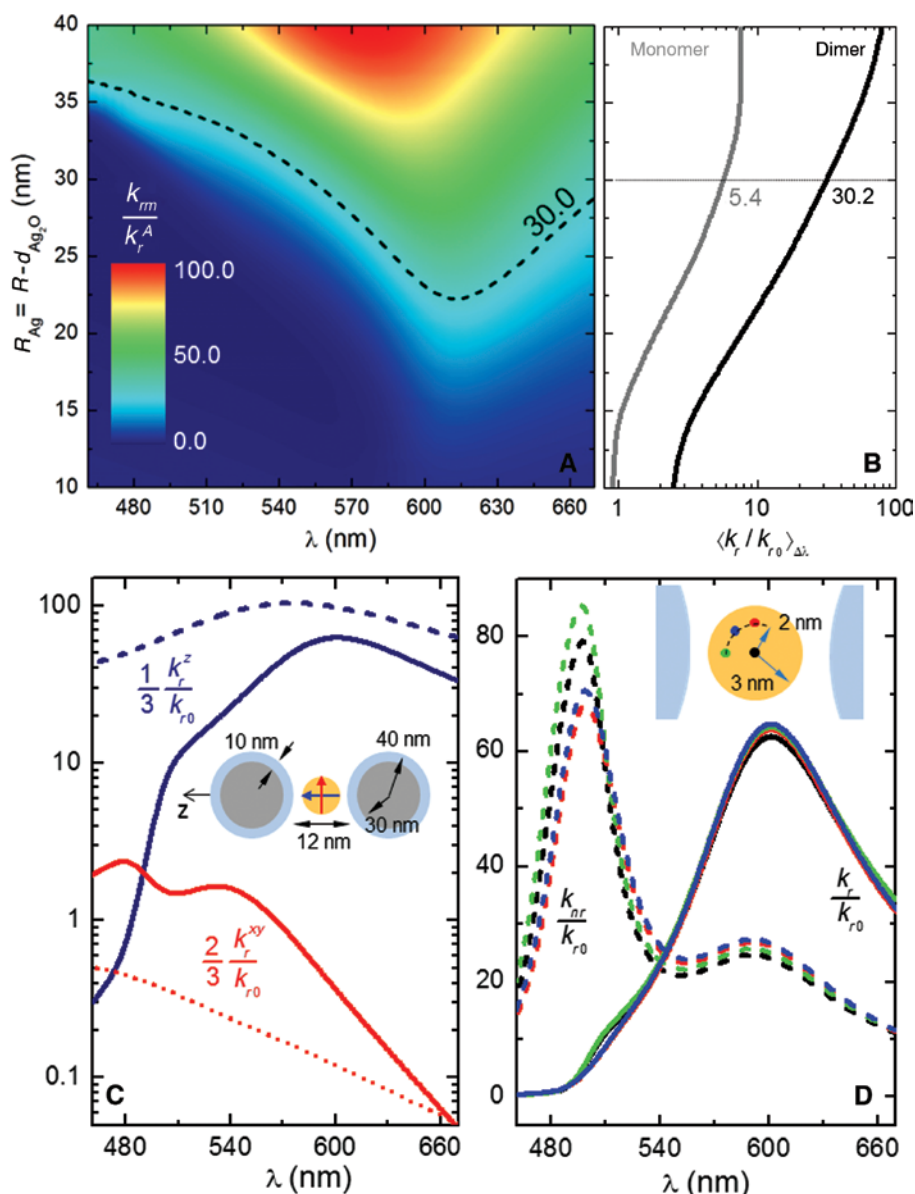


Figure 3: Simulated rate dependencies.

(A) Normalized radiative decay rate as a function of wavelength and NP oxidation level. Black dashed line renders the contour $k_r/k_{r0} = 30$. (B) Spectrally averaged decay rate as a function of oxidation level for monomers (grey) and dimers (black). (C) Radiative decay for both axial (dark blue) and normal (red) fluorophore orientations for non-oxidized (dashed lines) and oxidized (solid lines) dimers. The inset shows a sketch of the OA geometry. (D) Radiative and non-radiative decay rate for four different fluorophore positions (colors, see inset) within the DNA origami between an oxidized NP dimer.

approaches to extract changes of the radiative rate require fluorescence lifetime measurements [12], which are difficult due to the strong lifetime reduction of dyes in the dimer antennas.

We have performed numerical simulations in order to gain insight into our experimental findings. We use the fact that the number of photons emitted before photobleaching in the three experimental configurations (origami reference, monomer, and dimer) can be expressed as follows [9, 18]:

$$\langle n \rangle = \frac{Q_r}{Q_b} = \frac{k_r}{k_r + k_{nr} + k_b} \cdot \frac{k_r + k_{nr} + k_b}{k_b} = \frac{k_r}{k_b}, \quad (3)$$

where $Q_r = \frac{k_r}{k_r + k_{nr} + k_b}$ and $Q_b = \frac{k_b}{k_r + k_{nr} + k_b}$ are the fluorescence emission yield and bleaching yield, respectively, with k_r , k_{nr} , and k_b as the radiative, non-radiative, and bleaching rates, respectively. Due to the Purcell effect, k_r varies from one structure to the other [19], whereas k_b is inherent to the fluorophore itself (the same in all cases). Thus, we

can identify the ratio between average photons emitted in different samples (accessible experimentally) with the ratio between the corresponding radiative decay rates (calculated numerically). Like in the measurements, the decay rate in the absence of metal NPs, k_{r0} , is taken as the reference in the simulations. Mimicking the experimental conditions, $k_r(k_{r0})$ is obtained by computing the power radiated by the source in the presence (absence) of the silver NPs and within an NA = 1.4 solid angle along the vertical direction.

Special efforts were devoted to mimicking the experimental set-up and samples as accurately as possible in our theoretical model. The DNA origami and metal NPs are placed on top of a silica substrate (with refractive index $n_{\text{SiO}_2} = 1.5$) [20] and embedded in an aqueous environment ($n_{\text{H}_2\text{O}} = 1.33$) [21]. The origami was modeled as a 6-nm-diameter, 110-nm-height cylinder with homogeneous refractive index $n_{\text{origami}} = 2.1$ [22]. The frequency-dependent silver permittivity for the $R = 40$ -nm radius NPs was fitted to the experimental data [23]. In accordance with recent theoretical reports, nonlocal effects in the metal permittivity were neglected [24]. The plasmonic monomer and dimer were attached to the DNA origami 60 nm above the silica substrate in a similar way as sketched in Figure 1. The refractive index of the ssDNA surrounding the NPs was approximated to the refractive index of the buffer, $n_{\text{H}_2\text{O}}$ [25].

Previous simulations of Au dimer structures [26] predict significantly higher enhancement of the radiative rate, over two orders of magnitude. We ascribe the mismatch with our results to the oxidation of silver. We therefore modeled the oxidized NPs through a core-shell geometry with a silver inner core of radius R_{Ag} and an outer Ag_2O layer of thickness $d_{\text{Ag}_2\text{O}}$ and refractive index $n_{\text{Ag}_2\text{O}} = 2.5$ [27]. Figure 3A shows the normalized radiative decay rate, k_r/k_{r0} , for the dimer structure within the spectral window $\Delta\lambda$ corresponding to the emission band of Alexa488 as a function of the level of NPs oxidation. The spectra were obtained by averaging the fluorophore orientation, $k_r = \frac{1}{3}k_r^z + \frac{2}{3}k_r^{xy}$, where z -direction is defined parallel to the dimer axis. In all cases, the decay rate spectra are governed by a broad maximum that originates from the dipolar plasmonic resonance supported by the OA at $\lambda \sim 550$ – 600 nm. Note that this peak lowers, broadens, and redshifts slightly with increasing $d_{\text{Ag}_2\text{O}}$. The black dashed line renders the contour $k_r/k_{r0} = 30$ (the measured radiative enhancement factor). Our results indicate that significant OA oxidation must be introduced in the numerical calculations in order to reproduce the experimental results. This fact is further clarified in Figure 3B, which renders the spectrally averaged radiative enhancement factor

$$\langle k_r/k_{r0} \rangle_{\Delta\lambda} = \frac{1}{\Delta\lambda} \int_{\Delta\lambda} (k_r/k_{r0}) d\lambda, \quad (4)$$

which accounts for the spectral emission range of the fluorophore employed. We find that a 10-nm oxide layer leads to values for this averaged magnitude, which are in agreement with experiments for both monomers (5.4) and dimers (30.2).

Figure 3C plots the two contributions to the total decay rate for a non-oxidized (dashed lines) and an oxidized (solid lines) dimer. The latter presents a 10-nm-thick oxide layer, the configuration closer to the experimental results in Figure 3B. The inset in Figure 3C shows the system geometry and fluorophore orientations, parallel (blue) and normal (red) to the OA axis. We can observe that the parallel contribution completely governs the spectra, although the contribution due to normal orientation increases slightly in the oxidized case. Finally, Figure 3D shows the little dependence of k_r/k_{r0} on the fluorophore position within the bulk of the DNA origami. The radiative decay rate evaluated at three different positions (green, blue, and red lines) was displaced 2 nm from the origami center (black line) overlap. We have also calculated the corresponding non-radiative decay rates, which vary more significantly in space. These spectra show a narrow peak at shorter wavelengths ($\lambda \sim 490$ nm) compared with the radiative ones. This is caused by the excitation of a higher order, quadrupole-like, dark plasmonic resonance in the dimer. We can observe that the non-radiative decay channel becomes faster as the fluorophore approaches one of the metal NPs, in agreement with recent theoretical reports on emitter-plasmon strong coupling in dimer geometries [28].

3 Conclusion

We have studied the effect of OAs on the photostability of single fluorophores. We exploited the DNA origami technique to self-assemble OAs consisting of one (monomer) and two (dimer) 80-nm Ag colloidal NPs and a single Alexa488 fluorophore in the 12-nm gap between the NPs with nanometer precision and stoichiometric control. For monomer structures, we obtained an enhancement factor of the average number of emitted photons of $4\times$ in agreement with previous measurements. Dimer structures yielded an order of magnitude higher enhancement of the photostability, reaching a factor of $30\times$. To the best of our knowledge, this represents the highest average photon enhancement reported to date determined at the single

molecule level with homogenous structures. Finally, these results are rationalized with the aid of numerical simulations. The experimental results of monomers and dimers are only matched when the oxide layer surrounding the NPs is considered. In both cases, similar thickness of oxide layer was determined, indicating the validity of the model. In contrast to the oxide layer, changing fluorophore position around the OA hotspot had a negligible effect.

4 Materials and methods

Eighty-nanometer silver NPs were purchased from BBI Solutions (Cardiff, UK) and functionalized with thiolated single-stranded DNA oligonucleotides (Ella Biotech GmbH, Planegg, Germany) according to Ref. [29]. DNA origami pillar folding, sample preparation, and epifluorescence wide-field imaging are described elsewhere [17]. The excitation intensity at 487 nm was set to be fivefold higher for reference measurements than for monomer and dimer measurements in order to bleach the molecule in about the same time. Single-molecule videos were recorded for 500 frames at 100-ms integration time and an electron multiplying gain of 10. For analysis, a custom-written LabVIEW software (National Instruments Corporation, Austin, TX, USA) was used. Only molecules with single-step photobleaching transients were selected and background corrected by the bleached intensity level. The number of photons for each molecule was calculated by integrating the whole intensity transient. For each sample (reference, monomer, and dimer), photon numbers were plotted in a histogram and fitted exponentially to obtain the mean number of photons from the decay constant.

Numerical simulations were performed using COMSOL Multiphysics™ (Burlington, MA, USA), a numerical solver of Maxwell's equations based on the finite element method. In the radiative enhancement calculations, the flow of the far-field time-averaged Poynting vector across a large numerical aperture was computed ($NA \sim 1.3$ in agreement with the experimental conditions). The non-radiative spectra were obtained from the power dissipated within the metallic regions, as optical losses were neglected in the rest of materials. Our simulation scheme is similar to the one detailed in Ref. [30].

Acknowledgments: We acknowledge funding by a starting grant (SiMBA, EU 261162) of the European Research Council (ERC) and the Deutsche Forschungsgesellschaft (AC 279/2-1 and TI 329/9-1). IK is grateful for the support by the Mobility Plus grant 1269/MOB/IV/2015/0 from

the Polish Ministry of Science and Higher Education (MNiSW). CV thanks a scholarship of the Studienstiftung des deutschen Volkes. AIF-D and AC-G acknowledge funding from the Spanish MINECO under Contracts FIS2015-64951-R and MDM-2014-037716-4, respectively. AIF-D also acknowledges funding from EU Seventh Framework Programme under Grant Agreement FP7-PEOPLE-2013-CIG-630996. GA and PT acknowledge funding of the state ministry for research of lower saxony in the frame of the “Quantum- and Nanometrology” (QUANOMET) strategic research area. Quanomet is part of the LUH-TUBS research alliance.

Author contributions: The manuscript was written through contributions of all authors. All authors have given approval to the final version of the manuscript.

References

- [1] Drexhage KH. Interaction of light with monomolecular dye layers. *Prog Opt* 1974;12:163–232.
- [2] Li J-F, Li C-Y, Aroca RF. Plasmon-enhanced fluorescence spectroscopy. *Chem Soc Rev* 2017;46:3962–79.
- [3] Anger P, Bharadwaj P, Novotny L. Enhancement and quenching of single-molecule fluorescence. *Phys Rev Lett* 2006;96:113002.
- [4] Taminiau TH, Stefani FD, van Hulst NF. Enhanced directional excitation and emission of single emitters by a nano-optical Yagi-Uda antenna. *Opt Express* 2008;16:10858–6.
- [5] Kinkhabwala A, Yu Z, Fan S, Avlasevich Y, Mullen K, Moerner WE. Large single-molecule fluorescence enhancements produced by a bowtie nanoantenna. *Nat Photon* 2009;3:654–7.
- [6] Raab M, Vietz C, Stefani FD, Acuna GP, Tinnefeld P. Shifting molecular localization by plasmonic coupling in a single-molecule mirage. *Nat Commun* 2017;8:13966.
- [7] Curto AG, Volpe G, Taminiau TH, Kreuzer MP, Quidant R, van Hulst NF. Unidirectional emission of a quantum dot coupled to a nanoantenna. *Science* 2010;329:930–3.
- [8] Wientjes E, Renger J, Cogdell R, van Hulst NF. Pushing the photon limit: nanoantennas increase maximal photon stream and total photon number. *J Phys Chem Lett* 2016;7:1604–9.
- [9] Pellegrotti JV, Acuna GP, Puchkova A, et al. Controlled reduction of photobleaching in DNA origami–gold nanoparticle hybrids. *Nano Lett* 2014;14:2831–6.
- [10] Kéna-Cohen S, Wiener A, Sivan Y, et al. Plasmonic sinks for the selective removal of long-lived states. *ACS Nano* 2011;5:9958–65.
- [11] Punj D, Mivelle M, Moparthy SB, et al. A plasmonic ‘antenna-in-box’ platform for enhanced single-molecule analysis at micromolar concentrations. *Nat Nano* 2013;8:512–6.
- [12] Holzmeister P, Pibiri E, Schmied JJ, Sen T, Acuna GP, Tinnefeld P. Quantum yield and excitation rate of single molecules close to metallic nanostructures. *Nat Commun* 2014;5:5356.
- [13] Acuna GP, Bucher M, Stein IH, et al. Distance dependence of single-fluorophore quenching by gold nanoparticles studied on DNA origami. *ACS Nano* 2012;6:3189–95.

- [14] Acuna GP, Moller FM, Holzmeister P, Beater S, Lalkens B, Tinnefeld P. Fluorescence enhancement at docking sites of DNA-directed self-assembled nanoantennas. *Science* 2012;338:506–10.
- [15] Aissaoui N, Moth-Poulsen K, Kall M, Johansson P, Wilhelmsson LM, Albinsson B. FRET enhancement close to gold nanoparticles positioned in DNA origami constructs. *Nanoscale* 2017;9:673–83.
- [16] Lok CN, Ho CM, Chen R, et al. Silver nanoparticles: partial oxidation and antibacterial activities. *J Biol Inorg Chem* 2007;12:527–34.
- [17] Vietz C, Kaminska I, Sanz Paz M, Tinnefeld P, Acuna GP. Broadband fluorescence enhancement with self-assembled silver nanoparticle optical antennas. *ACS Nano* 2017;11:4969–75.
- [18] Hirschfeld T. Quantum efficiency independence of the time integrated emission from a fluorescent molecule. *Appl Opt* 1976;15:3135–9.
- [19] Giannini V, Fernández-Domínguez AI, Heck SC, Maier SA. Plasmonic nanoantennas: fundamentals and their use in controlling the radiative properties of nanoemitters. *Chem Rev* 2011;111:3888–912.
- [20] Malitson IH. Interspecimen comparison of the refractive index of fused silica. *J Opt Soc Am* 1965;55:1205–9.
- [21] Hale GM, Querry MR. Optical constants of water in the 200-nm to 200- μ m wavelength region. *Appl Opt* 1973;12:555–63.
- [22] Thacker VV, Herrmann LO, Sigle DO, et al. DNA origami based assembly of gold nanoparticle dimers for surface-enhanced Raman scattering. *Nat Commun* 2014;5:3448.
- [23] Palik ED. Handbook of optical constants of solids. New York, Academic Press, 1985.
- [24] Tserkezis C, Mortensen NA, Wubs M. How nonlocal damping reduces plasmon-enhanced fluorescence in ultranarrow gaps. *Phys Rev B* 2017;96:085413.
- [25] Elhadj S, Singh G, Saraf RF. Optical properties of an immobilized DNA monolayer from 255 to 700 nm. *Langmuir* 2004;20:5539–43.
- [26] Punj D, Regmi R, Devilez A, et al. Self-assembled nanoparticle dimer antennas for plasmonic-enhanced single-molecule fluorescence detection at micromolar concentrations. *ACS Photonics* 2015;2:1099–107.
- [27] Todisco F, D'Agostino S, Esposito M, et al. Exciton-plasmon coupling enhancement via metal oxidation. *ACS Nano* 2015;9:9691–9.
- [28] Li RQ, Hernangomez-Perez D, Garcia-Vidal FJ, Fernandez-Dominguez AI. Transformation optics approach to plasmon-exciton strong coupling in nanocavities. *Phys Rev Lett* 2016;117:107401.
- [29] Vietz C, Lalkens B, Acuna GP, Tinnefeld P. Functionalizing large nanoparticles for small gaps in dimer nanoantennas. *N J Phys* 2016;18:045012.
- [30] Liu M, Lee TW, Gray SK, Guyot-Sionnest P, Pelton M. Excitation of dark plasmons in metal nanoparticles by a localized emitter. *Phys Rev Lett* 2009;102:107401.

Supplemental Material: The online version of this article offers supplementary material (<https://doi.org/10.1515/nanoph-2017-0081>).